The mobility and relaxation kinetics of charge carriers in molecular materials studied by means of pulse-radiolysis time-resolved microwave conductivity: dialkoxy-substituted phenylene-vinylene polymers

2002 J. Phys.: Condens. Matter 14 9935

(http://iopscience.iop.org/0953-8984/14/42/308)

INSTITUTE OF PHYSICS PUBLISHING JOURNAL OF PHYSICS: CONDENSED MATTER

J. Phys.: Condens. Matter **14** (2002) 9935–9954 PII: S0953-8984(02)37214-4

The mobility and relaxation kinetics of charge carriers in molecular materials studied by means of pulse-radiolysis time-resolved microwave conductivity: dialkoxy-substituted phenylene-vinylene polymers

John M Warman, Gerwin H Gelinck and M P de Haas

Radiation Chemistry Department, IRI, Delft University of Technology, Mekelweg 15, 2629 JB, Delft, The Netherlands

Received 21 May 2002
Published 11 October 2002
Online at stacks.iop.org/JPhysCM/14/9935

Abstract

The information that can be obtained on the mobility and relaxation kinetics of electronic charge carriers in bulk molecular materials using the pulse-radiolysis time-resolved microwave conductivity technique is illustrated by results on several dialkoxy-substituted phenylene-vinylene polymers. The results demonstrate the sensitivity of the electronic properties of such conjugated polymers to their morphology. Thus, despite having the same conjugated backbone, the mobility and the relaxation kinetics (due to trapping and/or charge recombination) depend strongly on the nature of the alkyl-chain substituents, with in particular a marked difference between symmetrically and unsymmetrically dialkoxy-substituted compounds. For the latter, high-temperature annealing has a substantial positive effect on the mobility and lifetime of mobile carriers. The mobilities found for annealed materials range from a low of 0.0025 $cm^2\ V^{-1}\ s^{-1}$ for the methoxy, ethyl-hexoxy derivative, MEH-PPV, to a high of 0.036 $cm^2\ V^{-1}\ s^{-1}$ for the di-octadecoxy derivative, $(OD)_2$-PPV. The latter compound becomes a free-flowing liquid above 190 °C but still displays a high charge-carrier mobility of 0.017 $cm^2\ V^{-1}\ s^{-1}$. For all compounds the temperature dependence of the mobility after annealing is only slight over the range from −50 to +150 °C with an energy of activation <0.1 eV. Saturation of vinylene residues (breaking the conjugation) results in a marked decrease in the mobility. For very high accumulated doses of radiation the mobility on a nanosecond timescale remains unaffected but the decay of the mobile carriers at longer times becomes faster. This effect is completely reversed on annealing at 150 °C.

1. Introduction

The conventional experimental methods applied to the study of the semiconductive properties of molecular materials can be divided into four categories:

(1) chemical doping or continuous 'band-gap' illumination with measurement of the steady-state current [1–5],
(2) laser flash-photolysis with time-resolved detection of transient conductivity changes down to picosecond timescales [4–7],
(3) measurement of the current/voltage characteristics of charge injection devices [8, 9],
(4) time-of-flight (TOF) studies of charge-carrier drift in an electric field [2, 10–12].

All of these methods require the preparation of thin, preferably pinhole-free layers of the polymeric material, a few tens of microns thick at most, to which electrode contacts must be applied. While these restrictions are clearly similar to those also operative in the construction of electronic devices using this type of material and therefore may be considered to be more 'relevant', they are not conducive to the ready characterization and comparison of a variety of materials.

To circumvent some of the problems associated with DC conductivity techniques we have developed an electrodeless method of monitoring the conductivity of a material which can readily be applied to a variety of bulk solid samples: the pulse-radiolysis time-resolved microwave conductivity (PR-TRMC) technique [13–15]. In this method the material of interest is uniformly ionized with a short pulse of high-energy radiation. The high penetrating power and non-specific energy deposition characteristics of high-energy radiation make it possible to uniformly ionize samples several millimetres thick irrespective of their colour, chemical composition, and morphology and unaffected by scattering effects at domain or grain boundaries. In addition, the energy per unit volume deposited in the material can be accurately measured by dosimetry.

A change in the conductivity of the medium resulting from the radiolytic formation of mobile charge carriers is measured as a change in the power level of microwaves which propagate through the sample. Knowing the energy deposited in the sample, the maximum concentration of charge-carrier pairs formed during the pulse can be estimated with reasonable accuracy. This allows in turn estimates to be made of the *minimum* value of the sum of the charge-carrier mobilities from the end-of-pulse conductivity. The actual value of the mobility is expected to be no more than an order of magnitude higher than this minimum value.

Because of the ultrahigh frequencies (GHz) and low field strengths (about 10 V cm^{-1}) used, the mobility values obtained should be free from grain and domain boundary effects and will reflect mainly the mobility of charge carriers within well-organized (i.e. high-mobility) domains within the material. The use of nanosecond time resolution ensures in addition that in most cases the charge carriers are probed prior to their diffusional drift to intrinsic chemical or physical trapping sites. The mobility values determined should therefore be close to the optimum 'trap-free' values which could be achieved in a DC experiment with well-organized domains between the electrodes. In one of the few cases where a direct comparison of mobilities determined by PR-TRMC and by TOF measurements has proven to be possible (on a well-organized, discotic liquid-crystalline material), the agreement has been found to be very good [16].

It is worth pointing out a common mistake made in the discussion of mobility values determined using high-frequency, AC techniques. This revolves around the frequently asked question 'how far does a charge carrier move within one half period of the field oscillation?' The mobility value, μ, is then taken to determine this distance as $\mu E/2f$ which leads to

unrealistically small estimates, considerably less than atomic dimensions. The mobility however is a property of a large ensemble of charge carriers and cannot be applied to the motion of an individual carrier. The influence of a low-level electric field (i.e. $E\lambda \ll kT$ with λ the scattering length or jump distance) is to induce a small perturbation in the normal, isotropic diffusional motion of the ensemble. In the case of diffusion by one-dimensional hopping for example, this results in a *slight preference* for jumps in the direction of the field rather than the normal 50/50 statistics. It is this preferential motion of a small fraction of the carriers in an ensemble which results in a net drift velocity or displacement current. This is observed as a compensating current in the external circuitry of a DC experiment or as an attenuation in the case of an electromagnetic wave propagating in the material. The mistake made in the above calculation for AC fields is similar to concluding that in a TOF measurement all of the charge carriers are moving in the direction of the electric field with a velocity μE whereas, of course, close to half of them are moving in the opposite direction at any given time, for non-dispersive transport at moderate field strengths.

In addition to information on the mobilities of charge carriers, derived from the end-of-pulse conductivity, information on the localization and recombination processes occurring subsequent to their formation can be obtained from the after-pulse decay of the conductivity. Due to the non-perturbative nature of the probing field, the decay kinetics is free of problems associated with medium polarization and field-induced drift to domain boundaries or electrode interfaces which can dominate the relaxation kinetics of the conductivity in time-resolved DC measurements.

In what follows the application of the technique and the type of information that can be obtained are illustrated by results obtained on dialkoxy-substituted phenylene-vinylene polymers. Some of the results have been previously reported [17, 18]. Recent results in which PR-TRMC is applied to other π-conjugated polymers in the bulk [19–24] and in solution [25, 26], as well as to π-stacked discotic materials [27–30], are to be found in other publications. A variation of the technique using flash-photolysis to form charge carriers, FP-TRMC, has been developed for the study of thin films [31–35] and dilute solutions [36–38] of polymeric compounds.

2. Experimental details

2.1. Samples

The primary molecular structures of the polymers studied are shown together with their pseudonyms in figure 1. The synthesis and chemical characterization of the compounds have been described elsewhere [39]. The polymers were received as freshly precipitated materials: MEH-PPV from The Melville Laboratory for Polymer Synthesis, University of Cambridge, UK (supplied by Professor Holmes and Dr Hwang) and the remainder from Philips Research Laboratories, Eindhoven, The Netherlands (supplied by Dr Staring and Dr Schoo). The weight-average molecular weights, M_W, determined by gel-chromatography, were between 200 and 500 kDa with typical polydispersities of 2–3. In the case of the series of broken-conjugation polymers, dMOM-PPV(n), the fraction of saturated vinylidene residues, $1 - n$, was determined from the contribution of the ethylidene group protons in the ^{1}H NMR spectra. For the 'fully conjugated' polymer, denoted as dMOM-PPV(1), the ^{1}H NMR signals from the methoxyethylidene residues were below the detection limit of about 2%, indicating $n > 0.98$.

Samples were prepared by compressing the polymeric material into a rectangular cell using a close-fitting PTFE rod. The cell consisted of a 14 mm long piece of copper waveguide with an internal cross-section of 3.55×7.1 mm^2 which was closed at one end by a metal plate

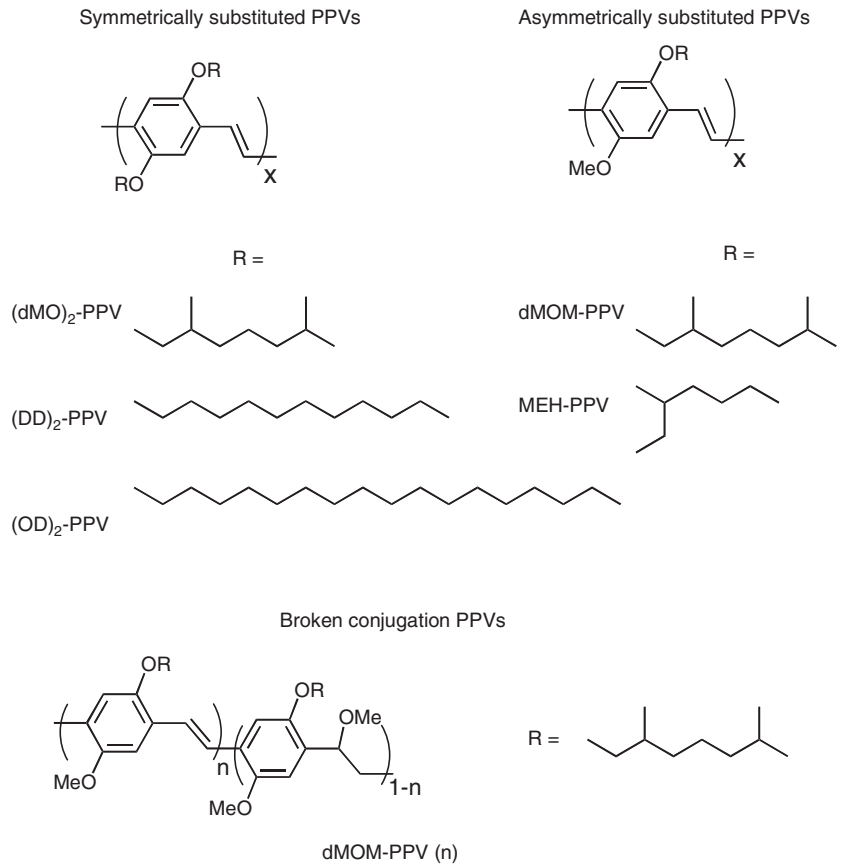

Figure 1. The molecular structures and pseudonyms of the dialkoxy-substituted phenylene-vinylene and phenylene-vinylene/ethylidene polymers studied.

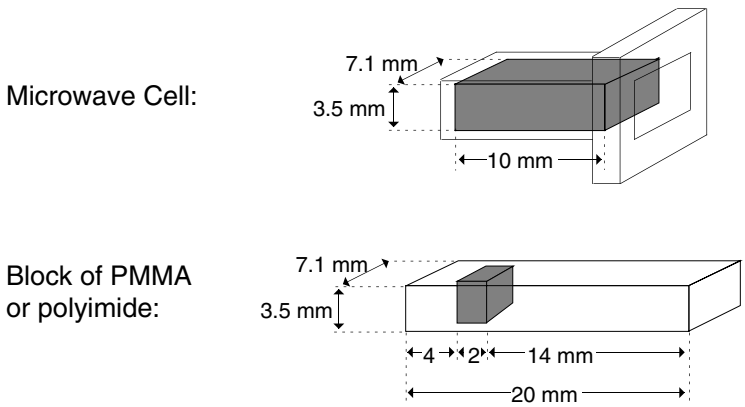

Figure 2. Upper: the Ka-band microwave cell into which a polymer sample of about 200 mg can be compressed. Lower: a PMMA or polyimide block into whose cavity a sample of about 20 mg can be compressed prior to insertion of the block into the microwave cell.

('short-circuit') and flanged at the other end for connection to the microwave circuitry; see figure 2. The cell was gold plated using Atomex solution (Engelhard Industries). The length (about 10 mm) and weight (about 200 mg) of the sample were accurately measured and used to calculate the fraction of the sample volume actually consisting of bulk solid, the filling factor F, taking a density of 1 g cm^{-3} for the solid. The value of F, which invariably lay between 0.6 and 0.8, was used to correct the radiation-induced conductivity for the fact that the sample volume was not completely filled.

When less material was available, ≈25 mg was compressed into a cavity of dimensions $6 \times 3 \times 2$ mm^3 in a PMMA or polyimide block as shown in figure 2. The blocks had outer cross-sectional dimensions slightly smaller than the inner dimensions of the waveguide cell into which they were inserted after filling. The block materials were chosen on the basis of their own extremely small radiation-induced conductivity.

The cell was attached to the waveguide circuitry inside a cryostat which was capable of covering a temperature range from −100 to +200 °C. The temperature was regulated by a thermocouple in contact with the cell. When a PMMA block was used the upper temperature was limited to 120 °C.

2.2. Pulse-radiolysis

The cell was irradiated with single pulses of 3 MeV electrons from a Van de Graaff accelerator. The pulses were quite square with rise and fall times of about 100 ps and a width which could be varied from 0.5 to 50 ns. The beam current could be varied but was usually kept close to 4 A, giving a range of integrated beam charge, Q, from 2 to 200 nC depending on the pulse width used. The value of Q was routinely measured during the course of a series of measurements by deflection of the beam onto a target connected to an electrometer.

To minimize attenuation in the copper cell wall, this was reduced in thickness to 0.4 mm on the incident broad-wall side. The penetration depth of 3 MeV electrons in materials of density 1 g cm^{-3} is about 15 mm. This is much larger than the sample thickness of 3.5 mm. In addition, the Gaussian half-width of the beam cross-section was larger than the lateral dimensions of the sample, thus ensuring close-to-uniform energy deposition and ionization of the material within the cell [15].

Dosimetry within the cell was carried out at regular intervals using Far West Technology-92 radiochromic dosemeter films. The dose D (in units of Gy = J kg^{-1}) was related to the integrated beam charge, which was simultaneously measured, to yield the parameter $[D/Q]$ Gy nC^{-1}. The energy deposited per unit volume in the polymeric material for a given pulse, D_v J m^{-3}, is the relevant dosimetry parameter in the present work and is given by

$$D_v = \rho Q[D/Q] \tag{1}$$

with ρ the density in kg m^{-3}. A typical value of $[D/Q]$ was close to 1×10^3 Gy nC^{-1} which for a 50 ns, 4 A pulse would result in $D_v = 2 \times 10^5$ J m^{-3} in 1 g cm^{-3} material.

If E_p is the average energy in electron volts required per ionization event, then the total concentration of charge-carrier pairs formed within a pulse, $N_p(0)$ m^{-3}, will be given by

$$N_p(0) = D_v/eE_p \tag{2}$$

with e the elementary charge (1.6×10^{-19} C). The value of E_p for high-energy radiation has been found to be given to a good approximation by the (semi)empirical expression derived by Alig *et al* [40]:

$$E_p \approx 2.73 \times E_I + 0.5. \tag{3}$$

In (3), E_I is the minimum energy required for ionization, i.e. the ionization potential for molecular materials or the band gap in the case of semiconductor materials. Perhaps

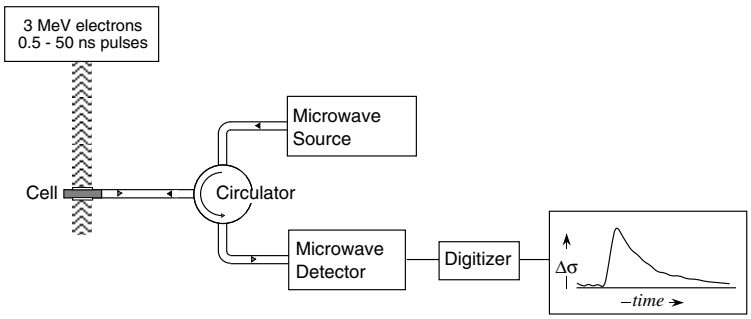

Figure 3. A very much simplified schematic representation of the PR-TRMC equipment. The 3 MeV electron pulses are provided by a Van de Graaff accelerator.

surprisingly, equation (3) is found to be quite universal, providing reasonable estimates of E_p for materials varying from low-band-gap semiconductors with E_I as low as 1 eV, to saturated hydrocarbon liquids for which E_I is closer to 10 eV. If a reasonably good estimate of E_I is available, then (3) should give a value of E_p which is good to within $\pm 20\%$. We emphasize that the concentration of charge-carrier pairs calculated on the basis of (2) using the value of E_p derived from (3) is the *maximum* concentration of initially formed charge carriers that could be present at the end of a pulse, i.e. in the absence of decay during the pulse via (geminate) recombination and/or trapping.

If a medium consists of different molecular components, the fraction of energy deposited initially in each component is proportional to its fractional contribution to the overall electron density of the medium, $\Delta Z/Z$. If the components differ in their E_p-values the average value of E_p will be given by

$$\langle E_p \rangle = 1 \Big/ \sum_n (\Delta Z\, E_p/Z)_n. \tag{4}$$

For example, for the present materials we can differentiate between the alkoxy side-chains with an E_I-value close to 8 eV ($E_p \approx 22$ eV) and the conjugated backbone with E_I close to 2.5 eV ($E_p \approx 7$ eV), i.e. taken to be close to the maximum of the first optical absorption band of dialkoxy-PPVs. The values of $\langle E_p \rangle$ calculated using (4) for the different polymers studied are listed in table 1 and are seen to vary from 13 to 18 eV. We can estimate the maximum possible concentration of initially formed charge-carrier pairs present at the end of a 50 ns, 4 A pulse taking a value of $\langle E_p \rangle = 15$ eV. This is about 10^{23} m^{-3} or 2×10^{-4} mol l^{-1}. Using this upper limit to the yield allows us to make lower-limit estimates of charge-carrier mobilities from the measured radiation-induced conductivity.

2.3. Time-resolved microwave conductivity

Any change occurring in the conductivity of the sample on pulse-radiolysis is monitored as a change in the microwave power reflected by the sample cell. A simple schematic drawing is shown in figure 3. Microwaves are generated by a Gunn oscillator with a tunable frequency range from 27 to 38 GHz and an average power level of about 100 mW. The microwaves are transmitted via a circulator to the sample cell where they propagate through the sample and are reflected at the end of the cell by the metal short circuit. The power level of 100 mW corresponds to a maximum electric field strength in the sample of about 10 V cm^{-1}. The reflected microwaves are directed by the circulator to one of two detectors which monitor the microwave power. One of these is a slow-response linear power meter for measuring the

Table 1. The effect of annealing at the temperature indicated for about 45 min on the radiation-induced conductivity of fully conjugated poly(phenylene-vinylene)s. All experimental values were measured at room temperature.

Polymer	Annealing temperature (°C)	E_p (eV)	$\Delta\sigma_{eop}/D$ (10^{-8} S m^2 J^{-1})	$\sum\mu_{min}$ (10^{-4} cm^2 V^{-1} s^{-1})
MEH-PPV	—	13	0.9	12
	150	13	1.9	25
dMOM-PPV(1.0)	—	13	1.5	18
	100	13	2.7	32
	150	13	6.7	80
$(dMO)_2$-PPV	—	15	9.1	140
	150	15	10.0	150
$(DD)_2$-PPV	—	16	6.1	100
	150	16	6.2	100
$(OD)_2$-PPV	—	18	11.0	200
	150	18	20.1	360

absolute microwave power and for calibration of the other detector which is a fast-time-response (about 1 ns) Schottky barrier diode (Alpha Industries 1N53B).

The output of the 1N53B diode is connected to a cascade of home-built impedance matching amplifiers (IMA) and a video amplifier of the Comlinear type CLC 100. The low-noise IMA has a frequency range of 10 Hz to 1 GHz and consists of two FETs of type ATF 21186 with a total amplification factor of 3. The GLC 100 has a frequency range from DC to 0.5 GHz and an amplification factor of 10. The amplifier output can be fed into either a Tektronix SCD 100 or TDS 680B digital oscilloscope for registration of transients on a linear time-base with an overall response time of about 1 ns. For longer times after the pulse a tandem combination of a Tektronix 2205 oscilloscope with a 7A13 plug-in and a Sony/Tektronix RTD 710 digitizer is used. This allows transients to be monitored from 10 ns to 1 ms on a pseudo-logarithmic time-base using a single pulse from the accelerator.

Apart from the digitizers, all active electronic components are contained in sheet-metal Faraday cages with special high-frequency EMI filtering devices for ventillation, power supply, and signal transmission. Only with such precautions can the high sensitivity of detection necessary be achieved. The noise level on the CW microwave power level on a nanosecond timescale is about 0.01%. The signal-to-noise sensitivity can be improved by averaging up to 32 individual transients.

2.4. Data analysis

In the present study only changes in the real component of the microwave conductivity (the imaginary or dielectric loss component of the permittivity) are measured. The change in reflected power, $\Delta P_R/P_R$, is directly related to the change in the conductivity of the sample for relatively small changes:

$$\Delta P_R/P_R = -A\,\Delta\sigma. \tag{5}$$

The sensitivity parameter A is an oscillatory function of the microwave frequency due to interference effects resulting from the similarity between the dimensions of the sample and the wavelength of the probing microwaves, about 3 mm. The value of A can be calculated on the basis of the known length of the sample and its 'effective' dielectric constant [13, 14]. TRMC transients are routinely taken over the available frequency range of 27–38 GHz in order

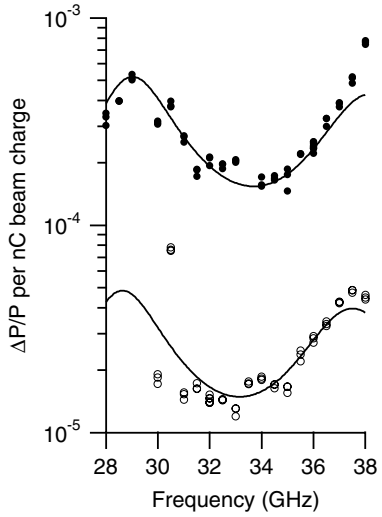

Figure 4. The frequency dependence of the end-of-pulse values of the dose-normalized change in microwave power reflected by a cell containing a sample of MEH-PPV (open circles) or $(OD)_2$-PPV (closed circles). The full curves are calculated dependences based on the length of the sample and a dielectric constant close to 2. The value of the dose-normalized conductivity is determined by the best fit over the frequency range to the absolute magnitude of $\Delta P/Q$.

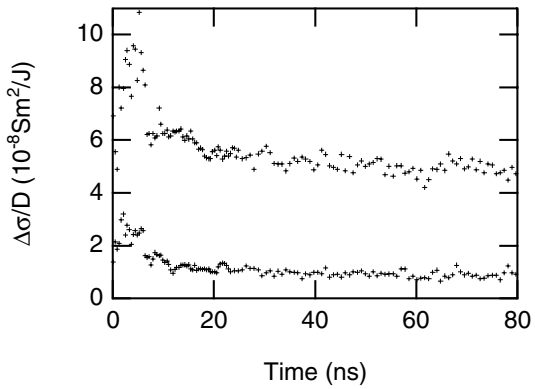

Figure 5. Dose-normalized conductivity transients obtained at room temperature on 5 ns pulsed irradiation of dMOM-PPV. Lower transient: freshly precipitated material. Upper transient: after annealing at 150 °C for 45 min. These transients were recorded using a transient digitizer with a 100 ps response time and a linear time-base.

to increase the accuracy of the value of $\Delta\sigma$ determined. Typical frequency scans of end-of-pulse conductivity signals together with calculated fits are shown in figure 4. The oscillatory behaviour is determined by the value of the dielectric constant of the medium and the absolute magnitude is determined by the value of the conductivity change.

The conductivity change at any time during or after the ionizing pulse is related to the concentration, N_i, and mobility, μ_i, of all charge carriers formed according to

$$\sigma(t) = e \sum_i N_i(t)\mu_i. \tag{6}$$

If no transformation or recombination of the initially formed, highly mobile primary charge carriers takes place during the pulse, then the end-of-pulse conductivity change will be given by

$$\Delta\sigma_{eop} = eN_p(0)[\mu(-) + \mu(+)] \tag{7}$$

$$= eN_p(0)\sum\mu. \tag{8}$$

We can take into account the possibility that primary charge carriers have (geminately) recombined or become trapped within the pulse by introducing the parameter, F_{eop}, which is simply the probability that initially formed charge carriers survive to the end of the pulse. F_{eop} is, in some ways, analogous to the quantum yield of charge separation in photoconductivity studies:

$$\Delta\sigma_{eop} = eN_p(0)F_{eop}\sum\mu. \tag{9}$$

Substituting for $N_p(0)$ from (2) in (9) and rearranging results in the following expression for the mobility sum in terms of the experimentally measurable parameter $[\Delta\sigma_{eop}/D_v]$,

$$\sum\mu = [\Delta\sigma_{eop}/D_v]E_p/F_{eop}. \tag{10}$$

Since the maximum value of F_{eop} is unity, a minimum value of the sum of the mobilities of the charge carriers can be determined from the radiation-induced conductivity

$$\sum\mu_{min} = [\Delta\sigma_{eop}/D_v]E_p. \tag{11}$$

The separate mobility values of the positive and negative charge carriers cannot be determined using the present technique.

The value of F_{eop} is determined to a large extent by the average thermalization distance of electrons from their sibling positive ion, $\langle r_{th}\rangle$, and the diffusional escape probability of charges separated by this distance. For irradiated organic materials, $\langle r_{th}\rangle$ has been found to be close to 50 Å and escape probabilities are usually between 1 and 10% at room temperature [41], even for low-dielectric-constant hydrocarbon media. In the present materials this thermalization distance is in fact longer than the interchain distance of at most 20 Å. There is therefore a high probability that the electron and 'hole' of an initial charge-carrier pair find themselves on different, widely separated polymer chains after thermalization. Because of this, we believe that the survival probability of initial charge carriers on a nanosecond timescale in the present type of medium will be at least 10% and possibly closer to unity. We consider it therefore extremely unlikely that the actual values of the mobility sum would be an order of magnitude larger than the values of $\sum\mu_{min}$ calculated as described above.

3. Mobilities

3.1. Room temperature (effects of annealing)

At an early stage in the investigation of conjugated polymeric materials it was observed that thermal annealing could result in a pronounced increase in the radiation-induced conductivity for certain compounds. An example of this is shown in figure 5 for dMOM-PPV. In this case the room temperature end-of-pulse conductivity increased by more than a factor of 4 after annealing the freshly precipitated material at 150 °C for 45 min. The results for all of the DA-PPV compounds are listed in table 1. As can be seen, annealing has a pronounced effect only for the unsymmetrically substituted compounds, suggesting that these are less well organized when freshly precipitated. Even after annealing the mobility for dMOM-PPV is substantially lower than for the symmetrically substituted $(dMO)_2$-PPV.

The zero-field DC hole mobilities for dMOM-PPV and $(dMO)_2$-PPV have been determined from the current–voltage characteristics of device structures with about 200 nm thick, spin-coated layers of the polymer between the electrode layers [42, 43]. The values found were about 1×10^{-7} and 1×10^{-5} $cm^2\ V^{-1}\ s^{-1}$ respectively. These values are orders

of magnitude lower than those of 0.8×10^{-2} and 1.5×10^{-2} cm^2 V^{-1} s^{-1} found in the present work and, although the trend is the same, the difference between the two compounds is much larger. This illustrates the much greater sensitivity to structural disorder of DC mobilities in which bulk drift of the carriers through the polymer layer is required.

Interestingly, the different effects of annealing and the ultimate values of the mobilities found in the present work can be related to the solubilities of the compounds. Thus, MEH is highly soluble even in benzene and displays no signs of aggregation. dMOM can be readily dissolved in hot benzene but eventually forms a gel on standing at room temperature. The symmetrically substituted compounds vary from very weakly soluble for $(dMO)_2$ and $(DD)_2$ to completely insoluble for $(OD)_2$. The differences in solubility can be understood in terms of the different propensities towards interchain π–π stacking which, if large, results in ready aggregation and insolubility. As a corollary of this, the freshly precipitated solids of those compounds with the lowest solubility would be expected to have the best structural organization in the solid phase and hence the highest charge mobility, as is found.

The absolute values of the mobilities, even after annealing, vary by more than an order of magnitude, from a low of 0.0025 cm^2 V^{-1} s^{-1} for MEH-PPV to 0.0360 cm^2 V^{-1} s^{-1} for $(OD)_2$-PPV. Since, as mentioned above, this trend appears to be related to the tendency towards interchain stacking, it might be inferred that interchain charge transfer makes an important contribution to overall charge transport, in the higher-mobility materials. This conclusion is however not necessarily correct since π-stacking also results in a more rigid and coplanar backbone structure which would also be expected to have a positive influence on intrachain charge migration. That $(OD)_2$-PPV has the highest mobility is not surprising in view of x-ray diffraction data which show that it forms a very well-organized, extended nematic liquid-crystalline phase [44]. As a result the material is quite malleable even at room temperature and at higher temperatures can be readily shear-oriented.

The one-dimensional intrachain hole mobility on isolated chains of MEH-PPV in dilute solution has been determined, also using the present technique, to be 0.43 cm^2 V^{-1} s^{-1} [25]. This corresponds to an isotropic value, as given in the present paper, of 0.14 cm^2 V^{-1} s^{-1}. This is a factor of more than 50 larger than the value found here for the bulk solid MEH-PPV even after annealing. This difference could be due to very rapid equilibrium trapping of charge carriers within the nanosecond duration of the pulse or to a high degree of static disorder in the backbone resulting in a very short coherence length in the bulk solid. In dilute solution, backbone disorder will be less effective in reducing the mobility because of the possibility of rapid conformational fluctuations.

The mobility found for bulk $(OD)_2$-PPV is only a factor of $\approx$4 lower than the isotropic, isolated chain value given above for MEH-PPV. This is within the possible order-of-magnitude difference between the actual $\sum \mu$ and $\sum \mu_{min}$ mentioned previously and could be due to an end-of-pulse survival probability smaller than unity. Unfortunately, because of its insolubility, a direct measurement of the isolated chain mobility could not be made for $(OD)_2$-PPV itself.

3.2. Effect of temperature

The dependence of $\sum \mu_{min}$ on temperature during the first heating of the freshly precipitated material from room temperature up to the annealing temperature of 150 °C and subsequent cooling is shown in figure 6 for the first four PPV derivatives in table 1. The data obtained on the cooling trajectories after annealing are plotted in an Arrhenius fashion in figure 7, except for $(DD)_2$-PPV which displays no temperature dependence within the errors of the measurements. The other three compounds show only a very weak temperature dependence with a tendency to approach a constant value below room temperature and to be slightly thermally activated above. The dotted straight lines in figure 7 correspond to an activation energy of 0.07 eV.

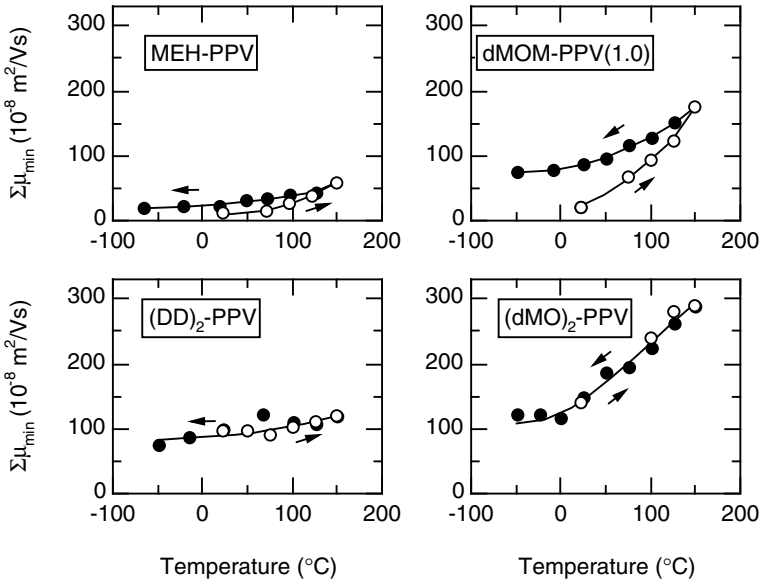

Figure 6. The temperature dependence of $\sum \mu_{min}$ for the polymers indicated on heating (open circles) and cooling (solid circles), beginning with the freshly precipitated samples.

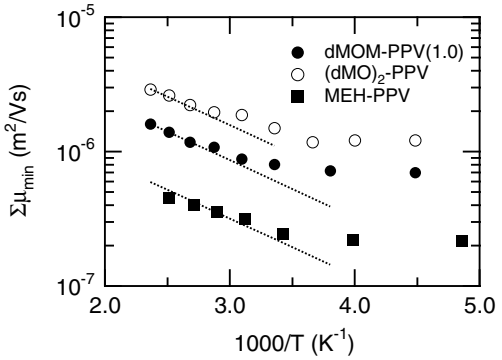

Figure 7. The temperature dependence of the mobility for the polymers indicated during cooling after annealing at 150 °C, plotted in an Arrhenius fashion. The dotted lines correspond to an activation energy of 0.07 eV.

3.3. Solid-to-liquid transition

$(OD)_2$-PPV is a particularly interesting compound since, as mentioned above, it is liquid crystalline and furthermore it undergoes a transition to an isotropic liquid phase just below 200 °C. Because of this the temperature dependence of $\sum \mu_{min}$ is more complex than for the other derivatives as shown in figure 8. On the first heating trajectory the mobility increases slightly up to a temperature of ≈190 °C, above which it abruptly decreases by close to 30%. This drop is clearly related to the transition to the isotropic liquid phase. The surprising aspect is that the decrease is in fact only 30%. The liquid is therefore almost as 'conductive' as the liquid-crystalline solid and displays a value of $\sum \mu_{min}$ (0.017 $cm^2\ V^{-1}\ s^{-1}$) which is even higher than for any of the other solid materials.

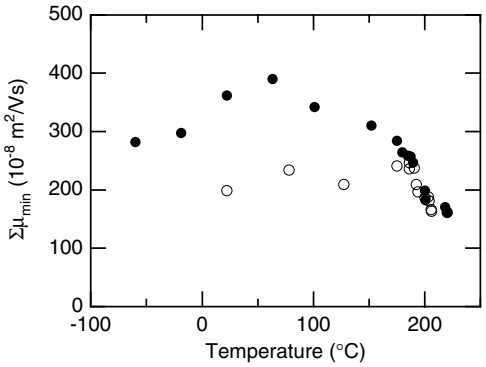

Figure 8. The temperature dependence of $\sum \mu_{min}$ for $(OD)_2$-PPV on heating (open circles) and cooling (solid circles) beginning with the freshly precipitated material. Above 190 °C this compound is a free-flowing liquid; on cooling it reverts to a nematic liquid crystal.

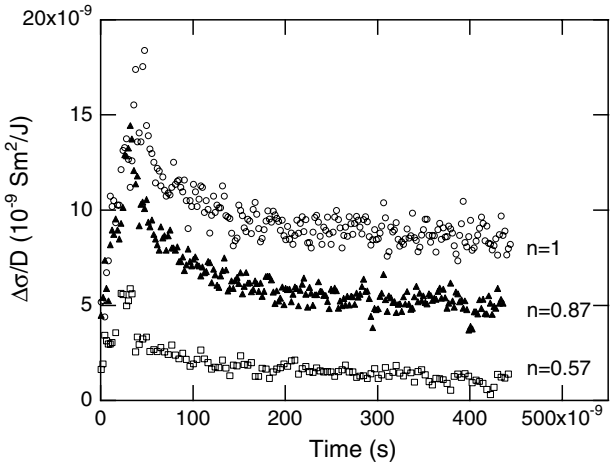

Figure 9. Dose-normalized radiation-induced conductivity transients obtained at room temperature for fresh samples of dMOM-PPV(n) polymers with $n = 1.0$, 0.87, and 0.57. From [17].

On cooling from the liquid phase the mobility increases by ≈30% at the liquid–liquid-crystal phase transition and then increases further on cooling, reaching a maximum value of close to 0.04 cm^2 V^{-1} s^{-1} at about 50 °C before eventually decreasing slightly with further decreasing temperature down to −60 °C.

3.4. Effect of broken conjugation

The negative influence of saturation of vinylidene residues on the mobility is shown in figure 9 by transients obtained for fresh samples of materials with different degrees of conjugation varying from nominally fully conjugated ($n > 0.98$) to $n = 0.57$. After the samples have been annealed, the differences are even greater than indicated by the transients shown in the figure. This is shown by the data in table 2 where the broken-conjugation compounds are seen to be relatively insensitive to annealing while the mobility in the fully conjugated polymer increases considerably.

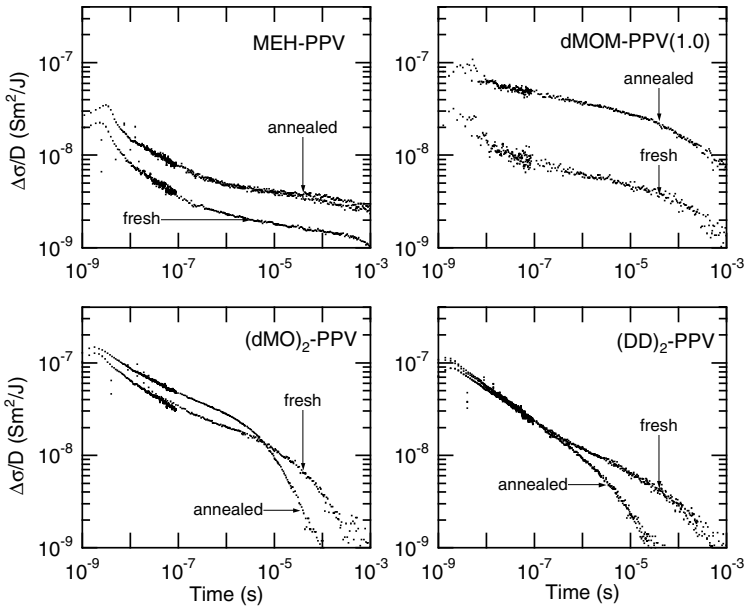

Figure 10. Single-pulse, radiation-induced conductivity transients from 1 ns to 1 ms taken at room temperature for the polymers shown before and after annealing for 45 min at 150 °C.

Table 2. The effect of broken conjugation on the radiation-induced conductivity of dMOM-PPV(n) polymers with n the degree of conjugation. All experimental values were measured at room temperature.

dMOM-PPV(n) n	Annealing temperature (°C)	E_p (eV)	$\Delta\sigma_{eop}/D$ (10^{-8} S m^2 J^{-1})	$\sum\mu_{min}$ (10^{-4} cm^2 V^{-1} s^{-1})
1.0	—	13	1.5	18
	100	13	2.7	32
	150	13	6.7	80
0.96	—	13	1.1	13
	100	13	1.5	18
0.87	—	13	0.9	11
	100	13	0.9	11
0.63	—	13	0.3	4
	100	13	0.4	5
0.57	—	13	0.3	4
	100	13	0.3	4

The zero-field DC hole mobilities for fully conjugated dMOM-PPV and a derivative with only 10% saturated vinylene residues (dMOM-PPV(0.9)) have been determined from the current–voltage characteristics of device structures with about 200 nm thick, spin-coated layers of the polymer between the electrode layers [43]. The values found were about 1×10^{-7} and 3×10^{-9} cm^2 V^{-1} s^{-1} respectively. As remarked previously, these values are orders of magnitude lower than the values found in the present work although the trend is the same.

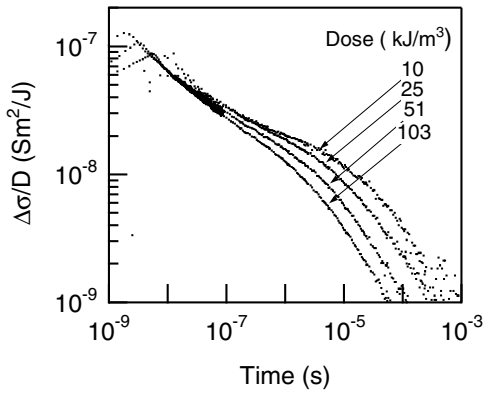

Figure 11. The effect of increasing the dose in the pulse (the end-of-pulse charge-carrier concentration) on the decay kinetics of the radiation-induced conductivity.

4. Decay kinetics

4.1. Effect of annealing

Subsequent to their formation, mobile charge carriers may decay by charge recombination or (temporary) localization at chemical or physical trapping sites within the medium. Both processes will result in a gradual decay of the radiation-induced conductivity. The decay kinetics in solid polymeric materials is in general extremely disperse, resulting in a gradual decrease in conductivity over several decades in time. The present compounds are found to be no exception, as illustrated by the transients in figure 10 which were obtained with single pulses using the logarithmic time-base over a time window from nanoseconds to a millisecond.

As for the mobility values discussed above, which were determined from the end-of-pulse conductivity, the effect of annealing on the decay kinetics differs from compound to compound. The lower-mobility MEH-PPV and dMOM-PPV compounds display an initial, more rapid decay over the first 100 ns which is less pronounced after annealing at 150 °C. For these materials there is an overall increase in the time over which the conductivity decays on annealing. For the symmetrically substituted compounds, while the initial decay is slightly extended, the decay at longer times actually becomes faster. As a consequence of these opposite effects of annealing, the dose-normalized conductivity is actually appreciably larger for the non-symmetrically substituted compounds at longer times.

A clue to the underlying reason for this unexpected behaviour is to be found in the dependence of the decay kinetics on the dose in the pulse, i.e. the initial concentration of charge carriers formed. This is discussed in the next section.

4.2. Effect of dose in the pulse (carrier concentration)

In the cases of MEH-PPV and dMOM-PPV the decay kinetics are found to be unaffected by increasing the dose in the pulse by an order of magnitude from about 10 to 100 kJ m^{-3}. For all three symmetric compounds however the decay becomes approximately tenfold faster at longer times. This is illustrated for $(dMO)_2$ in figure 11.

This increase in decay rate is reversible on returning to the lower dose and is not therefore a result of permanent radiation damage which will be discussed in a later section. It must therefore be due to homogeneous charge-carrier recombination, i.e. the recombination of positive and negative charge carriers with other than their initial geminate partner.

Homogeneous recombination requires that charge carriers of different pairs must be able to diffuse unhindered over relatively large distances in order to encounter each other. This requires the presence in the material of sufficiently large well-organized domains within which intermolecular charge transfer between different polymer chains can occur. An approximate estimate of the size of the domains required can be obtained by calculating the dimensions that would be necessary to form at least two pairs within the same domain for the lowest dose used.

A small-angle x-ray scattering study of $(OD)_2$ has shown the chains to be organized in a lamellar structure with the saturated hydrocarbon chains forming an 'insulating' layer between sheets of the π-stacked polymer backbones [44]. The minimum side, X m, of a square sheet of thickness, δ m, required for the formation of two charge-carrier pairs with a dose D_v, is given by

$$X > (2eE_p/\delta D_v)^{0.5}. \tag{12}$$

Since the sheets are $\approx$2 nm thick, X must be at least 0.5 μm in order to observe bimolecular recombination for a dose of 10 J m^{-3}.

The structure of the unsymmetrical compounds is unknown. However their macroscopic appearance is fibrous, indicating a one-dimensional underlying organization of the polymer chains. For the same domain size, X, a dose a factor of X/δ, i.e. more than two orders of magnitude, higher would be required to form multiple pairs for $\delta = 2$ nm. We consider that it is this difference in underlying organization that is responsible for the different dose dependences observed between the symmetrical and unsymmetrical derivatives.

4.3. Effect of temperature

A thorough study of the temperature dependence of the decay kinetics has only been carried out for the dMOM derivative. In figure 12 the change observed on decreasing the temperature from 150 °C, at which the sample had been annealed for 45 min, down to −50 °C is shown. The difference in form between the highest and the lowest temperature is seen to be considerable. For the former a shape resembling a stretched exponential decay is observed while for the latter an inverse power law dependence would better describe the time dependence, as seen by the close-to-linear decay in the log–log representation.

We have found that the conductivity decays can be fitted very well over the whole temperature range by empirically taking a rate coefficient for the disappearance of mobile charge-carrier pairs of the form $k/[1 + t/\tau]^n$, i.e.

$$\mathrm{d}N_p/\mathrm{d}t = -kN_p/[1 + t/\tau]^n. \tag{13}$$

The general solution for $n < 1$ is

$$N_p(t) = N_p(0)\exp\{-k\tau[(1 + t/\tau)^{(1-n)} - 1]/(1 - n)\}. \tag{14}$$

For times much longer than τ, equation (14) takes on the form of a stretched exponential, i.e.

$$N_p(t) = N_p(0)\exp\{-k\tau(t/\tau)^{(1-n)}/(1 - n)\}. \tag{15}$$

For the special case of $n = 1$, the solution to (13) is

$$N_p(t) = N_p(0)/[1 + t/\tau]^{k\tau}. \tag{16}$$

In this case, for times much longer than τ, the result is an inverse power dependence on time. The full curves in figure 12 were calculated using (14) and are seen to fit the data quite well. At present we are investigating the general applicability of this relationship and the possible physical significance of the three variable parameters k, τ, and n.

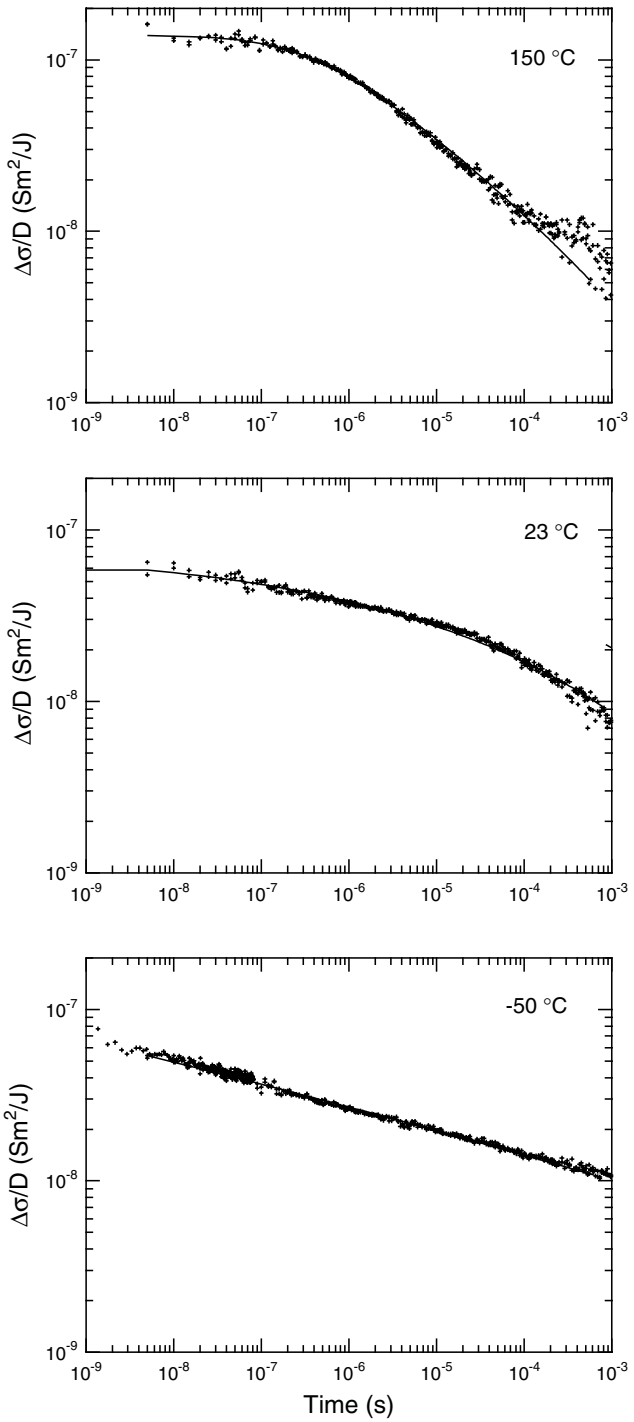

Figure 12. The effect of temperature on the decay kinetics of the radiation-induced conductivity of annealed dMOM-PPV. The full curves through the data points were calculated using equation (14). From [18]

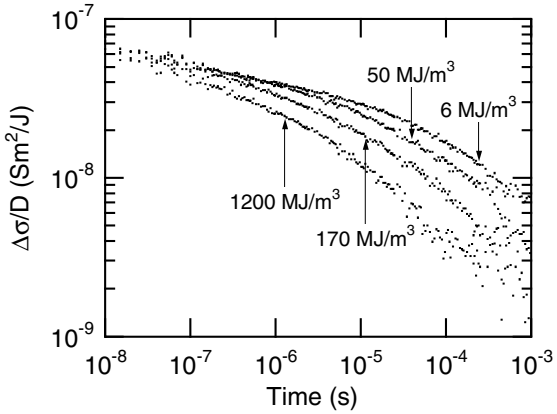

Figure 13. The effect of large accumulated doses of irradiation on the radiation-induced conductivity transients for dMOM-PPV. From [17].

4.4. Effect of accumulated dose (radiation damage)

The results reported in the previous sections were all obtained using the single-pulse mode of the accelerator with at most 32 pulses being averaged to improve the signal-to-noise ratio. The maximum accumulated dose during a series of measurements on a single sample was 2×10^7 J m^{-3} corresponding to ≈0.04 eV per monomer unit. No change in either the end-of-pulse conductivity or the decay kinetics could be detected over the course of the measurements.

Because of the importance of the degradation of polymeric materials in device applications, a study was carried out of the effect of much larger accumulated doses on the conductivity transients. This study was carried out at room temperature on the 150 °C annealed sample of dMOM-PPV in the following way. Single-pulse transients were first recorded for the previously unirradiated sample using as few pulses as possible. The sample was then subjected to repetitive pulsing at 10 Hz for a given length of time depositing about 10^4 J m^{-3} per pulse. Single-shot measurements were then repeated before applying a further train of repetitive pulses, and so on. The maximum accumulated dose was 1.2×10^9 J m^{-3}; about 4 eV per monomer unit.

The results are shown in figure 13. As can be seen, the value of the dose-normalized end-of-pulse conductivity was unaffected by the accumulated dose even up to the maximum used. The decay of the conductivity did however change, with the first half-life decreasing by a factor of ≈2 for a dose of 10^8 J m^{-3}. The first and second half-lives are plotted against accumulated dose in figure 14. For the largest dose, the first half-life was reduced by close to an order of magnitude and the second half-life by a factor of ≈30.

The effect on the decay kinetics was found to be completely reversed when the sample was annealed at 150 °C, as shown by the filled symbols above the arrows in figure 14. This result indicates that the defects produced by a high radiation dose do not involve permanent chemical change of the sample such as the oxidative formation of carbonyl groups or scission of vinylene residues as suggested to explain the degradation of samples on photolysis [45]. The most likely explanation is the gradual build-up of deeply trapped charge carriers which at sufficiently high concentration begin to act as recombination centres for the mobile carriers produced in subsequent single pulses. These ‘electronic’ defects can then be annealed out by inducing the recombination of the trapped charges at a high enough temperature in an analogous way to that occurring in thermoluminescence studies of irradiated solids.

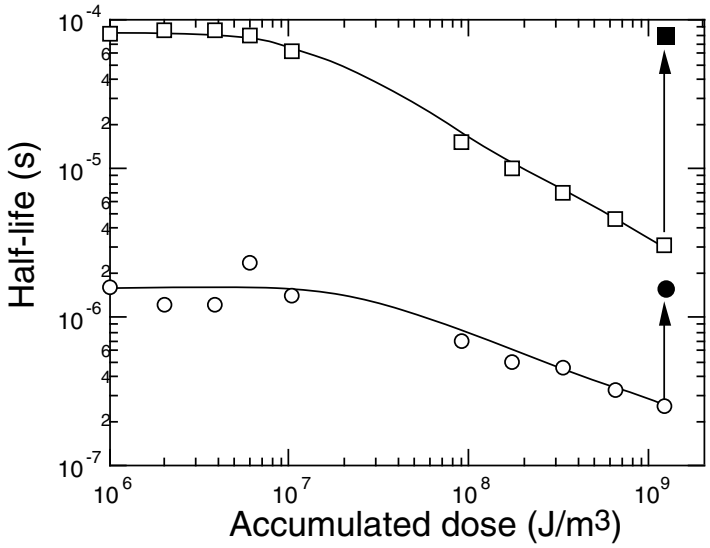

Figure 14. The first (circles) and second (squares) half-lives of the radiation-induced conductivity transients as a function of the accumulated dose of irradiation. The vertical arrows indicate the effect on the lifetimes of annealing the sample at 150 °C for ≈1 h after the maximum total dose. From [17].

5. Summary

5.1. Mobilities

As mentioned in the introduction, because of the short timescale of the measurements and the ultrahigh frequency of the electric field, the mobilities measured using the present technique may be considered to be trap-free values, free from the negative effects of barriers to transport at grain and domain boundaries. The values of $\sum \mu_{min}$ should therefore be close to the maximum values that could be achieved in DC experiments on the same material with well-organized single domains between the electrodes. We consider that mobility values more than an order of magnitude higher than these minimum values are unlikely.

In accordance with the above, estimates of the mobilities of charge carriers in PPV derivatives using DC techniques have been made which are orders of magnitude lower than the values of $\sum \mu_{min}$ found in the present work [10–12]. In most cases direct measurements using TOF methods have displayed only dispersive transport between the electrodes from which no definitive mobility values could be determined. Only in the case of the PPV derivative poly(1, 4-phenylene-1, 2-diphenyoxyphenyl vinylene), DPOP-PPV, could clear-cut drift times be determined from which a room temperature hole mobility of the order of 10^{-4} cm^2 V^{-1} s^{-1} could be estimated [10]. Much better-defined drift time data have been found for the ladder polymer MeLPPP which displays a propensity for self-organization [12, 46]. The room temperature hole mobility was accordingly found to be an order of magnitude larger than for DPOP-PPV and displayed only a weak dependence on temperature.

The large effect of structural order on the mobility of charge carriers is shown by our own results in the form of the substantial increases that can be induced by annealing at a high temperature and by the considerably range of values, from 0.0025 to 0.036 cm^2 V^{-1} s^{-1} even after annealing. The higher values are found for the symmetrically alkoxy-substituted

derivatives which display a greater tendency towards aggregation, an effect which has also been observed in device structures of the same materials [42, 43]. The degree of ordering for the dioctadecoxy derivative, which displays the highest mobility of all, is so great that it forms a liquid-crystalline solid phase.

In the case of MEH-PPV the mobility in the bulk solid phase is more than an order of magnitude lower than the value of the hole mobility of 0.43 $cm^2\ V^{-1}\ s^{-1}$ found for the isolated molecule in dilute solution [25]. This is ascribed to the fact that the structural disorder in the solid phase is static whereas in solution dynamic conformational fluctuations in the polymer backbone can more readily thermally activate charge migration. It is important in this regard that the solution experiments show that deep trapping at physical or chemical defects on the polymer chain itself does not occur.

The present results show that saturation of the vinylidene residues results in a marked reduction in the overall mobility, as might have been expected, and as has been found for device structures [43]. High doses of high-energy radiation, corresponding to about 4 eV per monomer unit, do not however decrease the mobility significantly although this does result in a decrease in the mobile carrier lifetime. The latter effect can be annealed out, indicating that it does not involve permanent chemical change but is probably due to the build-up of deeply trapped charge. This is in contrast to the high sensitivity of thin films of PPV derivatives to photolytic degradation in the presence of oxygen which leads to oxidative cleavage of the vinylidene residues [43].

5.2. Decay kinetics

The charge-carrier decay kinetics is for all of the materials studied highly dispersive. Here again large differences are found between the symmetrically and non-symmetrically substituted compounds with the decay becoming faster for the former and slower for the latter. In addition, the decay rate is found to increase with dose in the pulse for the former, indicating second-order charge recombination between charge-carrier pairs to occur, but is independent of dose for the latter. These differences are ascribed to differences in morphology between the compounds, with the symmetrical compounds having a two-dimensional, lamellar ordering and the non-symmetrical ones a more one-dimensional fibrous structure.

The temperature dependence of the decay kinetics, which was studied in detail for one of the compounds, shows a change from a stretched exponential to an inverse power law dependence on going from 150 to −50 °C. The data can be described over the whole temperature range using an empirical expression with a rate coefficient of the form $k/(1 + t/\tau)^n$.

Acknowledgments

The authors wish to express their thanks to Professor A B Holmes and Dr D-H Hwang (The Melville Laboratory for Polymer Synthesis, University of Cambridge, UK), and to Dr E G J Staring and Dr H F M Schoo (Philips Research Laboratories, Eindhoven, The Netherlands) for providing the polymer samples.

References

[1] Pichler K, Halliday D A, Bradley D D C, Burn P L, Friend R H and Holmes A B 1993 *J. Phys.: Condens. Matter* **5** 7155
[2] Gailberger M and Bässler H 1991 *Phys. Rev.* B **44** 8643
[3] Lee C H, Yu G and Heeger A J 1993 *Phys. Rev.* B **47** 15 543
[4] Lee C H, Yu G, Moses D and Heeger A J 1994 *Phys. Rev.* B **49** 2396

[5] Lee C H, Yu G, Sariciftci N S, Heeger A J and Zhang C 1995 *Synth. Met.* **75** 127
[6] Bradley D D C, Shen Y Q, Bleier H and Roth S 1988 *J. Phys. C: Solid State Phys.* **21** L515
[7] Moses D, Dogariu A and Heeger A J 2000 *Chem. Phys. Lett.* **316** 356
[8] Graupner W, Tasch S and Leising G 2000 *Semiconducting Polymers* ed G Hadziioannou and P F van Hutten (Weinheim: Wiley–VCH) ch 9
[9] Sirringhaus H *et al* 1999 *Nature* **401** 685
[10] Meyer H, Haarer D, Naarmann H and Hörhold H H 1995 *Phys. Rev.* B **52** 2587
[11] Obrzut J, Obrzut M J and Karasz F E 1989 *Synth. Met.* **29** E103
[12] Hertel D, Ochse A, Arkhipov V I and Bässler H 1999 *J. Imag. Sci. Technol.* **43** 220
[13] Infelta P P, de Haas M P and Warman J M 1977 *Radiat. Phys. Chem.* **10** 353
[14] Warman J M and de Haas M P 1990 *Pulse Radiolysis* ed Y Tabata (Boca Raton, FL: Chemical Rubber Company Press) ch 6
[15] Schouten P G, Warman J M and de Haas M P 1993 *J. Phys. Chem.* **97** 9863
[16] van de Craats A M, Warman J M, de Haas M P, Adam D, Simmerer J, Haarer D and Schuhmacher P 1996 *Adv. Mater.* **8** 823
[17] Gelinck G H and Warman J M 1996 *J. Phys. Chem.* **51** 20 035
[18] Gelinck G H, Warman J M and Schoo H F M 1998 *J. Radioanal. Nucl. Chem.* **232** 115
[19] Hoofman R J O M, van der Laan G P, Siebbeles L D A, de Haas M P, Bloor D and Sandman D J 2001 *Macromolecules* **34** 474
[20] Wegewijs B R, Grozema F C, Siebbeles L D A, de Haas M P and de Leeuw D M 2001 *Synth. Met.* **119** 431
[21] de Haas M P, van der Laan G P, Wegewijs B, de Leeuw D M, Baeuerle P, Rep D B A and Fichou D 1999 *Synth. Met.* **101** 524
[22] Hoofman R J O M, Siebbeles L D A, de Haas M P, Szablewski M and Bloor D 1999 *Synth. Met.* **102** 1417
[23] Schoonbeek F S, van Esch J H, Wegewijs B, Rep D B A, de Haas M P, Klapwijk T M, Kellogg R M and Feringa B L 1999 *Angew. Chem. Int. Edn* **38** 1393
[24] Wegewijs B, de Haas M P, de Leeuw D M, Wilson R and Sirringhaus H 1999 *Synth. Met.* **101** 534
[25] Grozema F C, Siebbeles L D A, Warman J M, Seki S, Tagawa S and Scherf U 2002 *Adv. Mater.* **14** 228
[26] Hoofman R J O M, de Haas M P, Siebbeles L D A and Warman J M 1998 *Nature* **392** 54
[27] van de Craats A M and Warman J M 2001 *Adv. Mater.* **13** 130
[28] van de Craats A M and Warman J M 2001 *Synth. Met.* **121** 1287
[29] van de Craats A M, Warman J M, Fechtenkötter A, Brand J D, Harbison M A and Müllen K 1999 *Adv. Mater.* **11** 1469
[30] van de Craats A M, Warman J M, Schlichting P, Rohr U, Geerts Y and Müllen K 1999 *Synth. Met.* **102** 1550
[31] Dicker G, Wegewijs B R, Piris J, Savenije T J, Huisman B H, de Leeuw D M, de Haas M P and Warman J M 2001 *Synth. Met.* **121** 1451
[32] Grozema F C, Savenije T J, Vermeulen M J W, Siebbeles L D A, Warman J M, Scherf U, Meisel A, Neher D and Nothofer H G 2001 *Adv. Mater.* **13** 1627
[33] Wegewijs B R, Piris J, Dicker G, Savenije T J, de Haas M P and Warman J M 2001 *Synth. Met.* **121** 1357
[34] Wegewijs B R, Dicker G, Piris J, Alba García A, de Haas M P and Warman J M 2000 *Chem. Phys. Lett.* **332** 79
[35] Savenije T J, Vermeulen M J W, de Haas M P and Warman J M 2000 *Sol. Energy Mater. Sol. Cells* **61** 9
[36] Hoofman R J O M, Gelinck G H, Siebbeles L D A, de Haas M P, Warman J M and Bloor D 2000 *Macromolecules* **33** 9289
[37] Gelinck G H, Piet J J, Wegewijs B R, Muellen K, Wildeman J, Hadziioannou G and Warman J M 2000 *Phys. Rev.* B **62** 1489
[38] Gelinck G H, Piet J J and Warman J M 1999 *Synth. Met.* **101** 553
[39] Holmes A B and Murray M M 2000 *Semiconducting Polymers* ed G Hadziioannou and P F van Hutten (Weinheim: Wiley–VCH) ch 1
[40] Alig R C, Bloom S and Struck C W 1980 *Phys. Rev.* B **22** 5565
[41] Nishikawa M 1991 *Handbook of Radiation Chemistry* ed Y Tabata, Y Ito and S Tagawa (Boca Raton, FL: Chemical Rubber Company Press) ch 7
[42] Martens H C F, Brom H B, Blom P W M and Schoo H F M 2000 *Phys. Status Solidi* **218** 283
[43] Martens H C F, Blom P W M and Schoo H F M 2000 *Phys. Rev.* B **61** 7489
[44] Picken S J 1998 private communication
[45] Cumpston B H and Jensen K F 1996 *Trends in Polymer Science* **4** 151
[46] Hertel D, Bässler H, Scherf U and Hörhold H H 1999 *J. Chem. Phys.* **110** 9214